NASA Technical Memorandum 106086
AIAA–92–2634

Surface and Flow Field Measurements in a Symmetric Crossing Shock Wave/Turbulent Boundary-Layer Interaction

D.O. Davis and W.R. Hingst
Lewis Research Center
Cleveland, Ohio

Prepared for the
10th AIAA Applied Aerodynamics Conference
sponsored by the American Institute of Aeronautics and Astronautics
Palo Alto, California, June 22–24, 1992

NASA

SURFACE AND FLOW FIELD MEASUREMENTS IN A SYMMETRIC CROSSING SHOCK WAVE/TURBULENT BOUNDARY LAYER FLOW

D. O. Davis* and W. R. Hingst*
NASA Lewis Research Center, Cleveland, Ohio

Abstract

Results of an experimental investigation of a symmetric crossing shock/turbulent boundary layer interaction are presented for a Mach number of 3.44 and deflections angles of 2,6,8 and 9°. The interaction strengths vary from weak to strong enough to cause a large region of separated flow. Measured quantities include surface static pressure (both steady and unsteady) and flowfield Pitot pressures. Pitot profiles in the plane of symmetry through the interaction region are shown for various deflection angles. Oil flow visualization and the results of a trace gas streamline tracking technique are also presented.

Nomenclature

α	=	shock generator plate deflection angle
δ_0	=	upstream B. L. thickness
D	=	width and height of wind tunnel (30.5 cm)
f	=	frequency (Hz)
$G(f)$	=	one-sided power spectrum
$L.E.$	=	leading edge
L_{gen}	=	length of shock generator plate
M	=	Mach number
P	=	static pressure
p	=	fluctuating component of static pressure
P_t	=	total pressure
P_{t2}	=	Pitot pressure
σ	=	RMS of fluctuating quantity
$T.E.$	=	trailing edge
v	=	volume (mole) fraction
x,y,z	=	cartesian coordinate system
x_{crs}	=	axial coordinate with origin at inviscid shock crossing location
xle, zle	=	position coordinates of generator plate leading edge
ρ	=	density

Subscripts

w	=	wall condition
0	=	upstream reference condition
∞	=	reference freestream condition

Introduction

ONE important class of shock/boundary-layer interactions is the glancing shock/turbulent boundary-layer interaction. This three-dimensional interaction occurs in many practical applications such as supersonic inlets, nozzle flows and supersonic combustors. The strong pressure gradients present in the interaction region create complex three-dimensional flows and can lead to flow separation. In some cases, two glancing shocks cross and produce a local region of strong adverse pressure gradient. This investigation focuses on crossing shocks of equal strength (symmetric) interacting with a turbulent boundary layer. Shown schematically in Fig. 1, this experimental configuration has the potential to provide good validation data for CFD methods. With a uniform incoming boundary-layer, the boundary conditions are relatively simple and well defined. In addition, for equal shock strengths the flow has a plane of symmetry reducing the required calculation volume. By varying the shock strengths, the interaction can be varied from weak to strong enough to cause separation.† The separated cases provide a particularly interesting test for CFD validation since the separation is not fixed by the geometry.

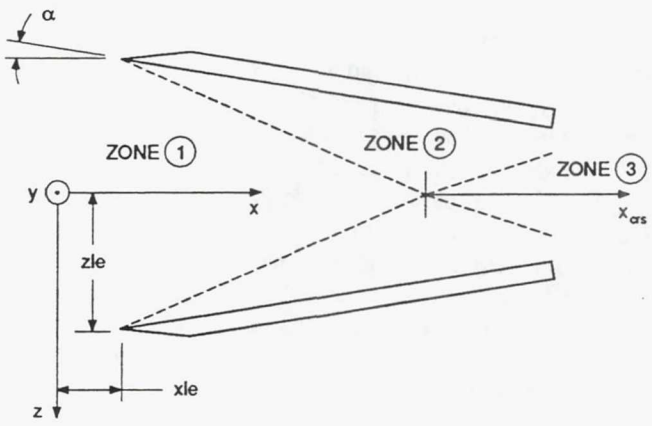

Fig. 1 Crossing shock wave/boundary-layer interaction with reference coordinates.

*Aerospace Engineer, Inlet, Duct, and Nozzle Flow Physics Branch, Member AIAA.

† As used in this paper, the term "separation" will refer to a distinct region of flow recirculation.

Table 1 Summary of previous experimental work.

Ref.	M_∞	Re' /m	Re_{δ_0}	δ_0 mm	α	x_{crs}/δ_0@T.E.
Mee *et al.*[1]	1.85	3.9×10^7	7.4×10^4	1.9	5°	3.8
Batcho *et al.*[2]	2.95	6.4×10^7	2.4×10^5	4.0	7° - 11°	16 - 21
Poddar *et al.*[3]	2.95	6.6×10^7	2.4×10^5	5.0	7°, 11°	16, 21
Hingst and Williams[4]	2.47 2.96 3.44 3.98	1.7×10^7 1.6×10^7 1.5×10^7 1.3×10^7	6.5×10^5 5.7×10^5 5.1×10^5 4.7×10^5	30.6 26.8 30.0 33.6	4,6,8,9° 4,6,8,10,11° 4,6,8,10,12° 4,6,8,10,12°	2.4 - 2.8 1.6 - 2.5 0.6 - 1.7 -0.3 - 1.0
Garrison and Settles[6]	2.96 3.83	8.6×10^7 7.9×10^7	2.6×10^5 2.4×10^5	3.0 3.0	7° - 13° 7° - 15°	8.6 - 14.8 -0.2 - 10.5
Kussoy and Horstman[7]	8.3	5.3×10^7	1.7×10^5	32.5	10°, 15°	1.0, 0.1

Previous experimental investigations of the equal strength crossing shock/boundary-layer interaction are summarized in Table 1. Some of these studies also considered unequal strength crossing shocks. Mee *et al.*[1] were the first to study the crossing shock interaction, providing mean surface static pressure data and limiting surface streamline patterns. Batcho *et al.*[2] provided similar data but also included preliminary measurements of the unsteady surface pressure and temperature along the plane of symmetry. These results showed that, unlike the data of Mee, for all deflection angles considered, the pressure rise downstream of the inviscid shock crossing location significantly exceeded (by as much as 50%) the theoretical inviscid shock pressure rise. Using the same facility as Batcho, Poddar *et al.*[3] mapped the unsteady surface pressure field. These measurements indicate that for stronger interactions, the flow downstream of the inviscid shock crossing position has a significant unsteady characteristic. Hingst and Williams[4,5] presented surface oil flow patterns and mean surface static pressure distributions over a relatively wide range of operating conditions. The first flowfield data for the crossing shock configuration was obtained by Garrison and Settles[6] who performed laser sheet flow visualization in the cross plane. From these results, a model of the complex shock structure through the interaction region was constructed. Most recently, Kussoy and Horstman[7] performed surface flow visualization, surface heat transfer and Pitot pressure measurements in the cross plane for hypersonic flow conditions.

Several of the experimental data sets have been used as a comparison to numerically generated results. Gaitonde and Knight[8] calculated the Mach 1.85, α= 5° interaction of Mee *et al.* Qualitatively, agreement with the experiment was good, but the calculations significantly overpredicted upstream influence and the rate of pressure rise along the plane of symmetry. Later, Gaitonde and Knight[9] numerically investigated a stronger symmetric crossing shock configuration (M=3, α=4° and 8°) as a means for controlling boundary layer separation, but no experimental data were available for comparison. Narayanswami *et al*[10] performed calculations based on the experimental configuration of Batcho and Poddar. Calculations were performed for M=2.95, α=9° and 11° utilizing both the algebraic turbulence model of Baldwin and Lomax[11] and the k-ϵ model of Jones and Launder[12]. Overall, the calculations with the algebraic model agreed fairly well with the experimental surface pressure data, but upstream influence was underpredicted. The k-ϵ calculations were considered preliminary and required further refinement. The data of Hingst and Williams[4,5] were recently used as a comparison for CFD calculations performed by Reddy[13] using the PARC3D code in conjunction with the Baldwin and Lomax turbulence model. The M=3.5, α=6° and 10° and M=4.0, α=6° cases were computed. The results of these calculations showed overall good agreement with the surface pressure data for both the unseparated and separated cases. For the separated case, however, the reverse flow region was predicted to be further upstream and larger than that observed experimentally.

A common feature of the crossing shock experiments is that, at the trailing edge of the generator plates, the flow encounters an expansion. The question then arises as to what degree does the upstream influence of the trailing edge expansion affect the interaction region. Clearly, if the expansion does feed upstream into the interaction region, it will tend to relieve the streamwise pressure gradient and thus the strength of the interaction. The distance between the shock crossing location and the generator plate trailing edge plane is a relevant parameter with regard to downstream influences. The last column

in Table 1 enumerates this distance normalized by the incoming boundary layer thickness for the various experimental studies. Of the studies where this parameter is relatively small, measured centerline static pressure was never observed to exceed that which is predicted by inviscid theory. The relatively large value of this parameter for the configuration tested by Batcho and Poddar correlates with the large centerline pressure rise above the inviscid value that they observed. One of the goals of this study is to examine the effect of varying this parameter by changing the generator plate length.

Experimental Program

Test Configuration

The present investigation was conducted in the NASA Lewis Research Center 1×1 ft. Supersonic Wind Tunnel. This wind tunnel is a continuous flow facility with Mach number variation provided by interchangeable nozzle blocks. The crossing shock/boundary-layer experiment is configured by using two shock generator plates that span the wind tunnel test section. The shock generators, when at angle of attack to the free stream tunnel flow, produce oblique shocks. The intersection of these shocks with the naturally occurring boundary-layer on the tunnel walls defines the experiment. A schematic of the test configuration with reference coordinates is shown in Fig. 1. With the exception of the shock generator plate lengths, the test hardware and actuation system for the present study is the same as was used by Hingst and Williams.[4] Deflection of the plates is accomplished by rotating the plates about a point. For reference, the position of the leading edge relative to the upstream reference plane (x=0) and the wind tunnel centerline (z=0) is given by the following (see Fig. 1):

$$xle(\text{cm}) = 6.350 - (9.525\sin\alpha + 3.810\cos\alpha) \quad (1)$$

$$zle(\text{cm}) = 15.875 - (9.525\cos\alpha - 3.810\sin\alpha) \quad (2)$$

Two sets of generator plates which are longer (L_{gen} = 22.9 cm and 25.4 cm) than the ones used by Hingst and Williams (L_{gen} = 20.3 cm) were fabricated in order to investigate how generator length affects the interaction region. The additional length is added to the generator plate trailing edge so that eqs. (1) and (2) are applicable for all plate lengths.

Results and Discussion

The initial plans for the test called for M_∞=3.44 and α=6° and 10°. These conditions were previously studied experimentally by Hingst and Williams[4] and numerically by Reddy[13] and correspond to unseparated and separated flow conditions, respectively. A significant difference, however, was that longer generator plates would be used in the present study to reduce the upstream influence of the trailing edge. To this end, the wind tunnel was initially configured with the 25.4 cm generator plates (the aforementioned studies considered 20.3 cm generator plates). At Mach 3.44, these plates were found to be good only up to deflection angles of 9°, after which the flow between the plates would completely unstart. With these plates, only surface static pressure and oil flow patterns were obtained for deflection angles between 2° and 9°. With the 22.9 cm plates installed, deflection angles up to 11° could be attained without a probe and up to 9° with a probe. It was then decided that the 22.9 cm plates would be used for flow field measurements, recognizing that 9° is the upper limit for deflection angle. Some limited data were also obtained at M_∞=2.96 for which the maximum deflection angle with a probe in the flow was determined to be 8°, but none is included in the present report.

Upstream Flow Conditions

The flowfield upstream of the generator plates was surveyed with a Pitot probe to insure that wind tunnel corner effects and the distorted boundary layers, which develop on the non-contoured wind tunnel nozzle walls, were bypassed behind the generator plates. Fig. 2 shows the results of the surveys plotted in terms of Mach number contours. The left and right sides of this figure correspond to M=2.96 and 3.44, respectively. Also indicated is the position of the shock generators at the largest deflection angle considered for each freestream condition. The upstream boundary layer was surveyed on the wind tunnel centerline (z=0) using a flattened Pitot probe. Various computed boundary layer parameters for the Mach 3.44 case are summarized in Table 2. The skin friction coefficient shown in the table was deduced from a curve fit of the data to the Sun-Childs[14] wall-wake profile. Analysis of the profile indicates that the boundary layer, which effectively begins at the wind tunnel nozzle throat and is not subjected to cross flow pressure gradients in the nozzle, can be characterized as uniform and in equilibrium.

Table 2 Upstream reference conditions (x=0).

M_∞	3.44
$P_{t,\infty}$ kPa	241.3
$P_{w,0}$ kPa	3.46
$T_{t,\infty}$ K	297.0
Re' /m	1.5×10^7
Re_{δ_0}	5.1×10^5
δ_0 mm	30.0
δ_0^* mm	10.7
θ_0 mm	1.4
$C_{f,0} \times 10^3$	1.18

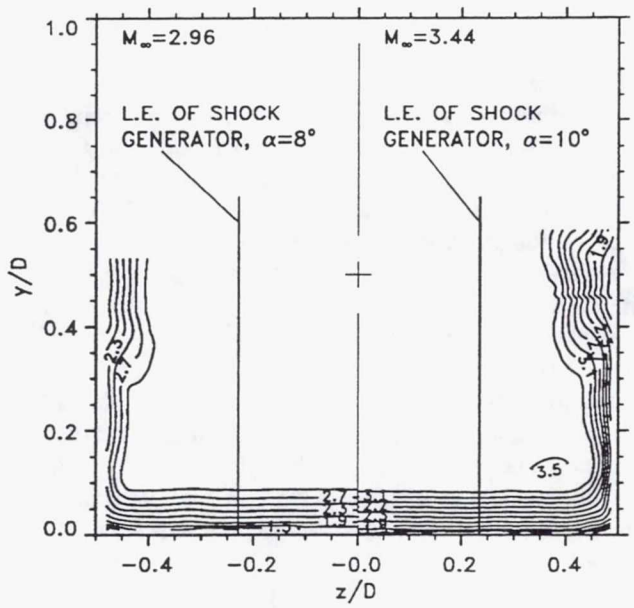

Fig. 2 Mach number contours at upstream station (x=0).

Flow Visualization

Near-wall limiting streamline behavior was investigated by means of oil flow visualization. A powdered fluorescent dye is mixed with 140 wt. oil and painted on the surface between the generator plates. The wind tunnel is then run until a steady pattern is established and then rapidly shut down to preserve it. Oil flow results were obtained for both the 22.9 cm and 25.4 cm plates. Three cases of strong interaction, i.e. the flow is separated, are shown Fig. 3. Fig. 3b shows the flow pattern for a deflection angle of 9° and a generator plate length of 22.9 cm. A significant separation region is clearly present. Other oil flow tests, which are not presented here, suggest that incipient separation occurs at approximately α=8° for the 22.9 cm long generator plates. Comparison between Fig. 3b and Fig. 3a shows the effect of increasing the deflection angle from 9° to 10°. The separation region increases in size and moves forward. An increase in deflection angle beyond 10° causes a complete unstart between the plates. Comparison between Fig. 3b and Fig. 3c illustrates the effect of increasing the plate length by 2.54 cm while maintaining the deflection angle at 9°. Although the strength of the shocks remain the same, the additional compression associated with the longer plates causes the separated region to move forward and grow in size.

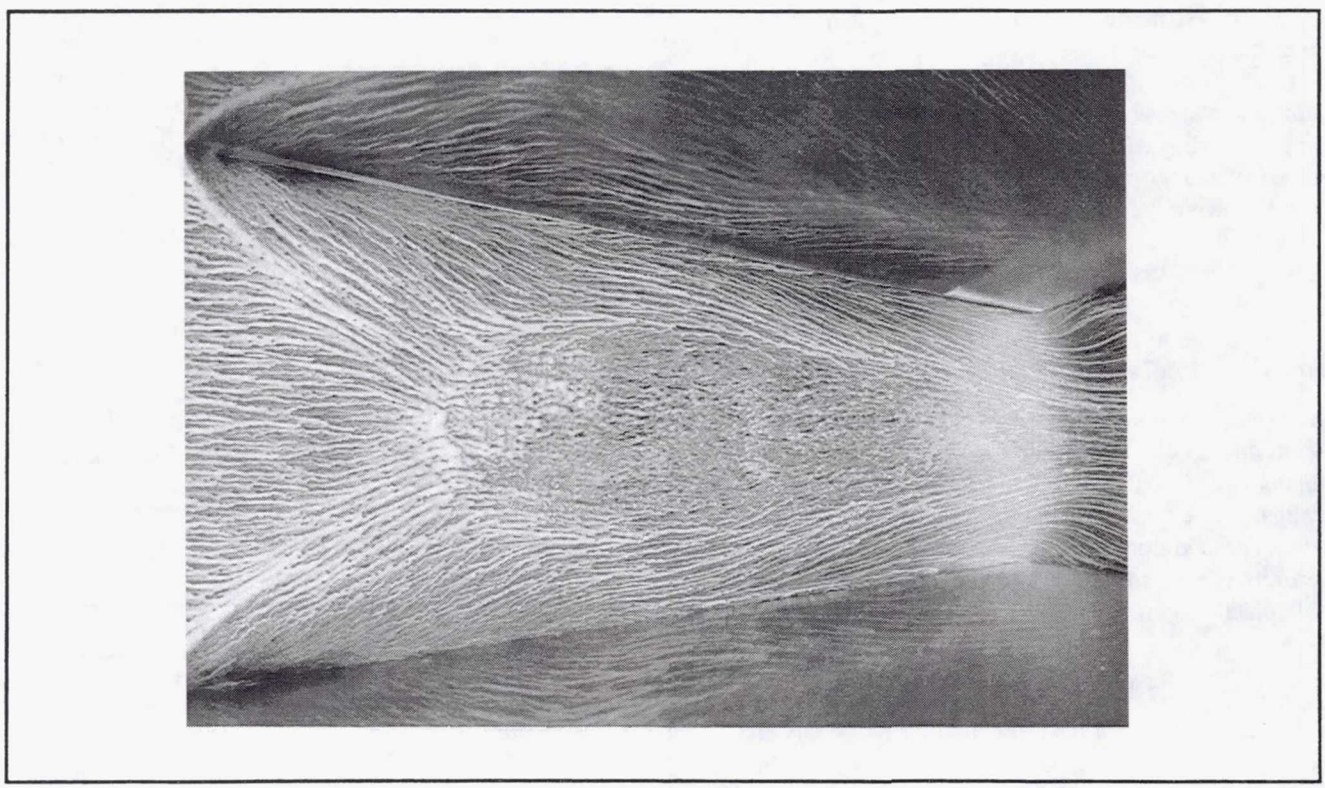

a) α=10°, L_{gen} = 22.9 cm.

Fig. 3 Surface oil flow patterns. (Continued . . .)

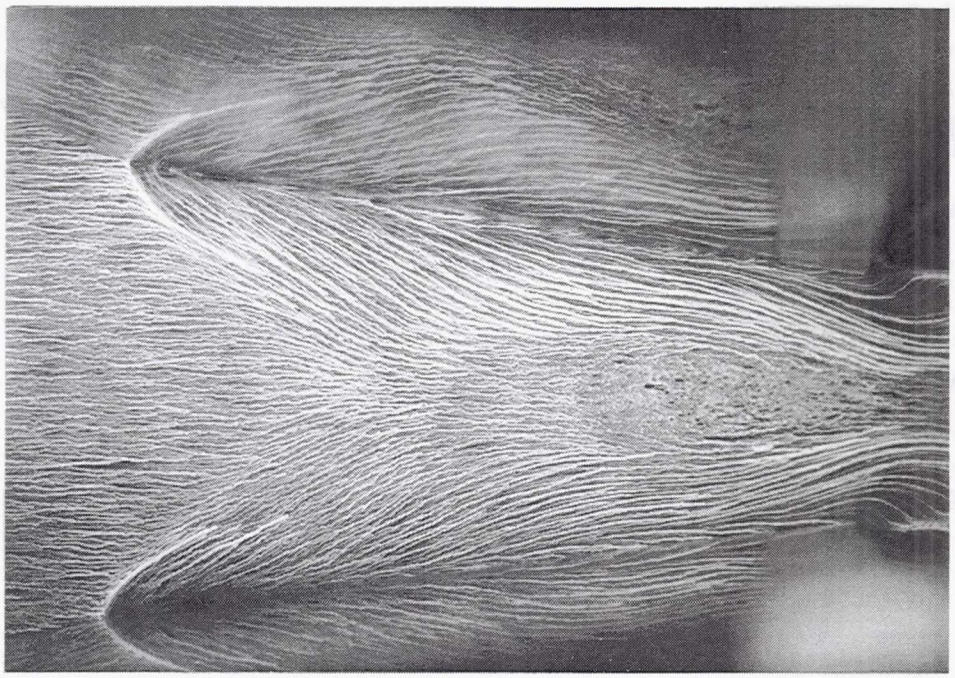

b) α=9°, L_{gen} = 22.9 cm.

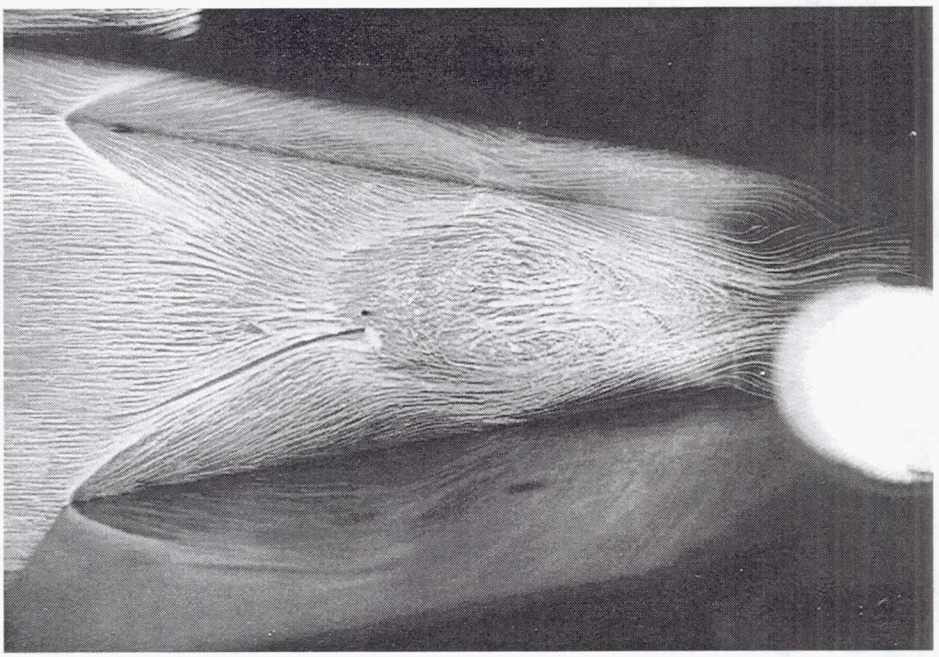

c) α=9°, L_{gen} = 25.4 cm.

Fig. 3 Surface oil flow patterns.

Mean Surface Static Pressure

Measurements of the mean surface static pressure over the entire surface between the generator plates were obtained using a repositionable plate with eighty 0.508 mm diameter taps. The plate could be installed in four different positions which yields a total of 320 taps. However, data from taps located under or behind the generator plates were discarded. The location of the pressure taps relative to the generator plates are shown in Fig. 2 of Ref. 5.

Contours of the surface static pressure for a Mach number of 3.44 and deflection angles between 2° and 10° are shown in Fig. 4. These data were obtained with the 22.9 cm plates with the exception of the lower right plot which corresponds to the 25.4 cm plates. The shaded regions indicate the approximate region of flow separation as deduced from the oil flow tests. The "×" symbols on the centerline indicate the positions of Kulite dynamic pressure transducers. From the results shown in Fig. 4, it is apparent that there is a qualitative difference between the pressure distributions for the unseparated and separated cases. Considering the surface pressure distribution along transverse lines (x=constant), it is seen that in the initial part of the interaction region for both cases, the minimum pressure occurs on the centerline (z=0). At a point upstream of the shock crossing location, a transition occurs whereby the centerline pressure becomes a maximum. For the unseparated cases, this behavior persists throughout the remainder of the interaction region. For the separated cases, however, a second transition occurs midway through the interaction such that the centerline pressure again becomes a minimum. This second transition, which is characterized by a transverse line of nearly constant pressure between the generator plates, correlates well with the location of the separation region. An examination of the oil flow and surface pressure distribution data for both the unseparated and separated cases of Hingst and Williams[4] reveals the same behavior for

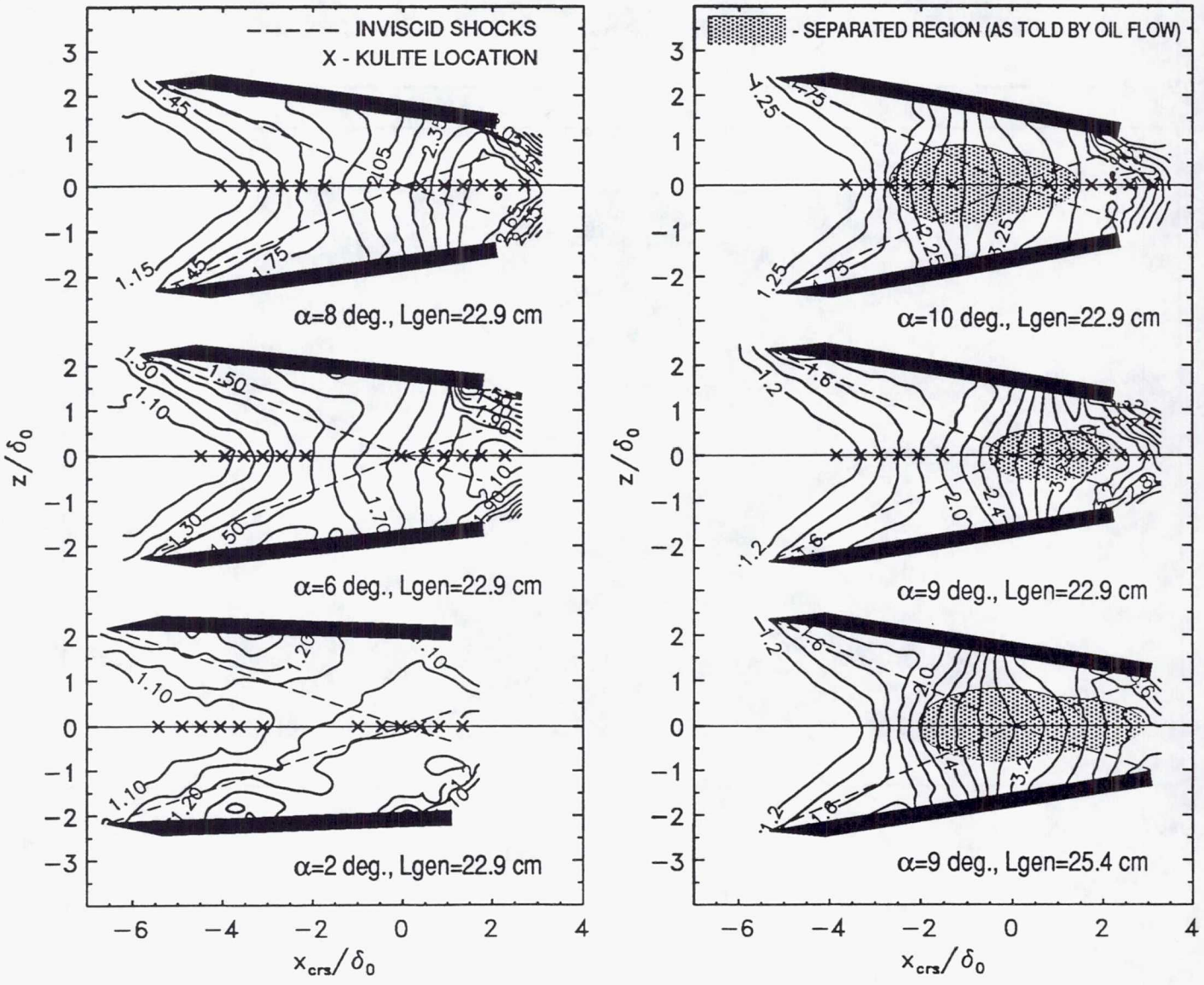

Fig. 4 Wall static pressure distributions.

the 20.3 cm plates. This distinguishing behavior between unseparated and separated flow conditions is also evident in the numerical calculations performed by Gaitonde and Knight.[9] Also, a comparison of the surface flow visualization and surface pressure presented by Batcho *et al.*[2], which for all cases were unseparated, agree qualitatively with the present unseparated cases. This observed difference in surface pressure behavior for the unseparated and separated cases may be useful as a means of detecting separation in symmetric crossing shock configurations.

Fig. 5 shows the surface pressure distributions in the plane of symmetry for both the 22.9 cm and 25.4 cm generator plates. Also, Hingst and Williams[4] data obtained with the 20.3 cm generator plates at Mach 3.44

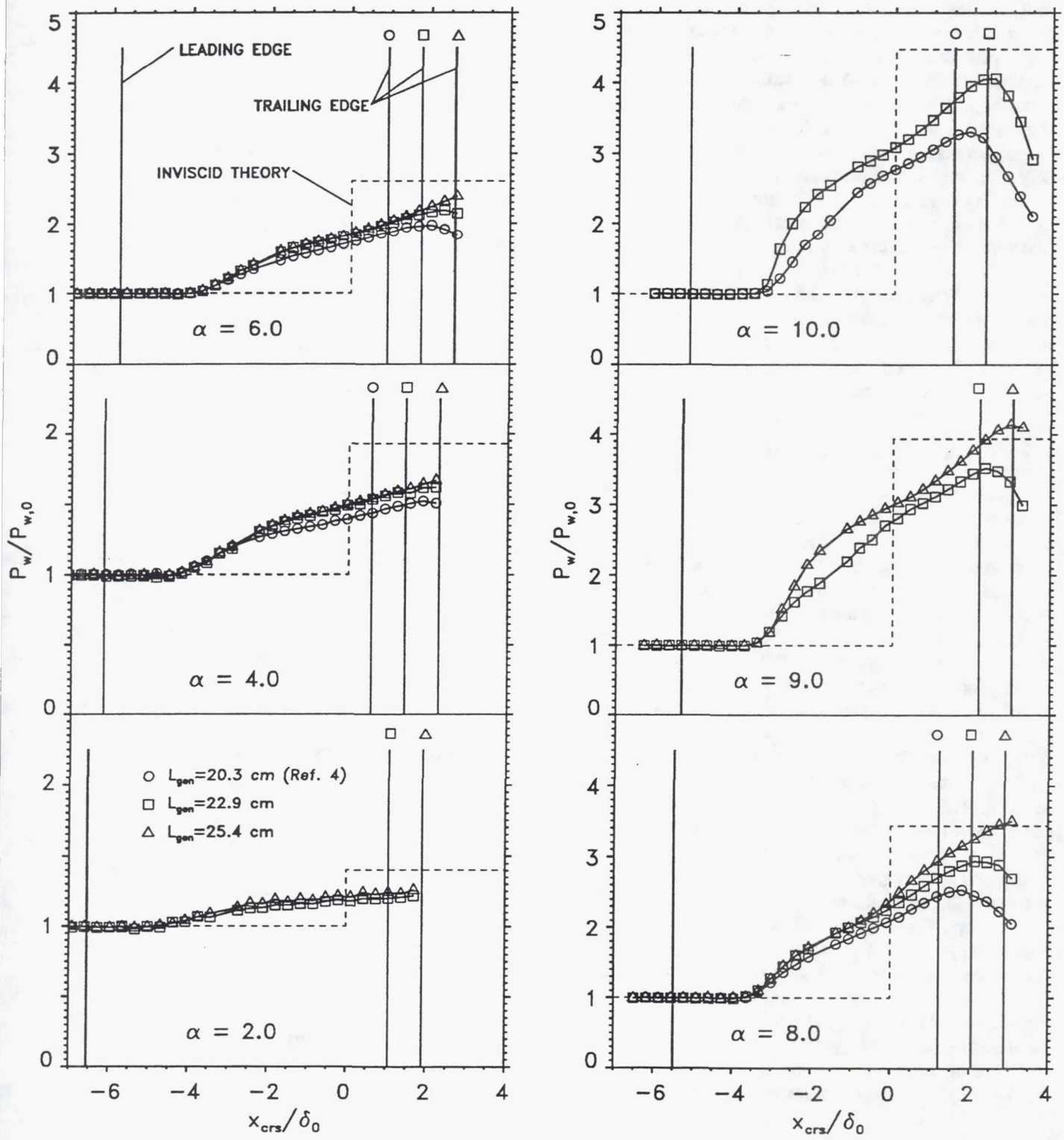

Fig. 5 Centerline wall static pressure distributions.

and α=4,6,8 and 10° are included for comparison. Note the scale change between α=4° and α=6°. At the weakest interaction, α=2°, there is little difference between the distributions corresponding to the two longest generator plates. At α=4°, data for the two longer plates again agree well with each other. However, the distribution corresponding to the 20.3 cm plates agrees with the longer plate data only for a short distance into the interaction region, after which the short plate data lie below the longer plate data. At α=6°, a similar trend is observed for the shortest plate, but also the distributions for the longer plates begin to deviate. Further increases in the deflection angle results in larger deviations for all plate lengths. We may conclude from these results that even for small deflection angles, the interaction region is influenced by the trailing edge expansion when the 20.3 cm plates are used. Indeed, even the longer plates appear to capture the true strength of the interaction only for the weaker cases. Achieving total isolation from the trailing edge expansion in a given facility may be difficult. To do so requires a relatively thin boundary layer which makes flow field measurements difficult. The presence of a trailing edge expansion does not invalidate a data set, but does require that it be modelled accurately in a CFD calculation.

Pitot Pressure Profiles in the Plane of Symmetry

Axial development of Pitot pressure profiles in the plane of symmetry are shown for α= 6, 8 and 9° in Figs. 6, 7 and 8, respectively. For these measurements, a single flattened Pitot probe was used with outer tip dimensions of 0.90 × 0.41 mm. The probe was inserted into the flow parallel to the generator plates from the wall opposing the interaction surface. Recall that all flowfield measurements were obtained with the 22.9 cm generator plates. The lower abscissa of the plots gives the axial location of the surveys relative to the inviscid shock crossing location and is normalized by the incoming boundary layer thickness. The upper abscissa is the survey location (in inches) measured from the upstream reference plane (see Fig. 1). At each axial profile station, the theoretical inviscid Pitot pressure is shown for comparison with the measured values. Scaling for the Pitot pressure is indicated (in kPa) above the upperleftmost profile. For reference, the wall static pressure is indicated on the plots in two ways. First, it is plotted as a limiting value to the Pitot surveys as the wall is approached (solid symbols), and second, the axial distribution of wall static pressure is overlaid (— – — line) and scaled as indicated by the right hand ordinate. Also indicated in these plots are the locations of the Kulite pressure transducers and the location of the trailing edge of the generator plates (T.E.). For α=9° (Fig. 8) the downstream region of the interaction could not be surveyed due to probe blockage causing the model to unstart. It should also be noted that the presence of the probe may affect the flowfield when the flow is separated or at near separation conditions. These effects, if any, are difficult to quantify.

Although the surveys were intended to pass directly from Zone 1 to Zone 3 through the shock crossing location (see Fig. 1), the results indicate that the actual axial traverse passed through a distance within Zone 2. This can be seen by examining the profiles immediately upstream and downstream of the inviscid shock crossing location. In the core region of the profiles, the Pitot pressure does not agree with either the Zone 1 or the Zone 3 theoretical values. In fact, they agree very well with the theoretical pressure in Zone 2. The axial extent of this deviation decreases with increasing deflection angle. The cause for the deviation is unknown, but may be related, at least in part, to probe deflection in the vicinity of the shock waves.

With reference to Fig. 6 (α=6° configuration), the shock induced pressure gradient creates two distinct features in the profiles. First, the deceleration of the near-wall flow produces an inflection point in the profiles, and secondly, this low momentum near-wall fluid acts as an obstacle to the upstream flow, spawning an oblique shock wave. The presence of the shock is embodied in a local rise in Pitot pressure above the core value. The origin of the shock is a coalescing of compression waves in the boundary layer and appears as a smooth bump rather than a discrete discontinuity. As it rises out of the shear layer, it becomes a more discernible step (see e.g., the profile at x=7.0 in). In Garrison and Settles'[6] model of the interaction, this shock is identified as the "centerline segment of the reflected separation shock" (segment "6a" in Fig. 12 of Ref. 6). For all profiles, the transverse gradient of the Pitot pressure at the wall always remains greater than zero ($\partial P_{t2}/\partial y > 0$) indicating that the flow does not separate. Increasing the deflection angle to α=8° (Fig. 7) produces similar results, but now the presence of the compression can be distinguished further upstream. Like the α=6° case, the gradient at the wall, although reduced, is non-zero throughout the interaction region. For α=9° (Fig. 8), the presence of the compression is observed even further upstream. The pressure gradient at the wall for this case appears to reach a zero value through a large portion of the interaction implying that the flow has separated. This region of zero gradient correlates well with the separated region observed in the oil flow results which are indicated in the figure by the shaded region. The step in the last axial survey is believed to be caused by an incipient unstart condition in the tunnel inasmuch as moving the probe further downstream resulted in a complete unstart of the model.

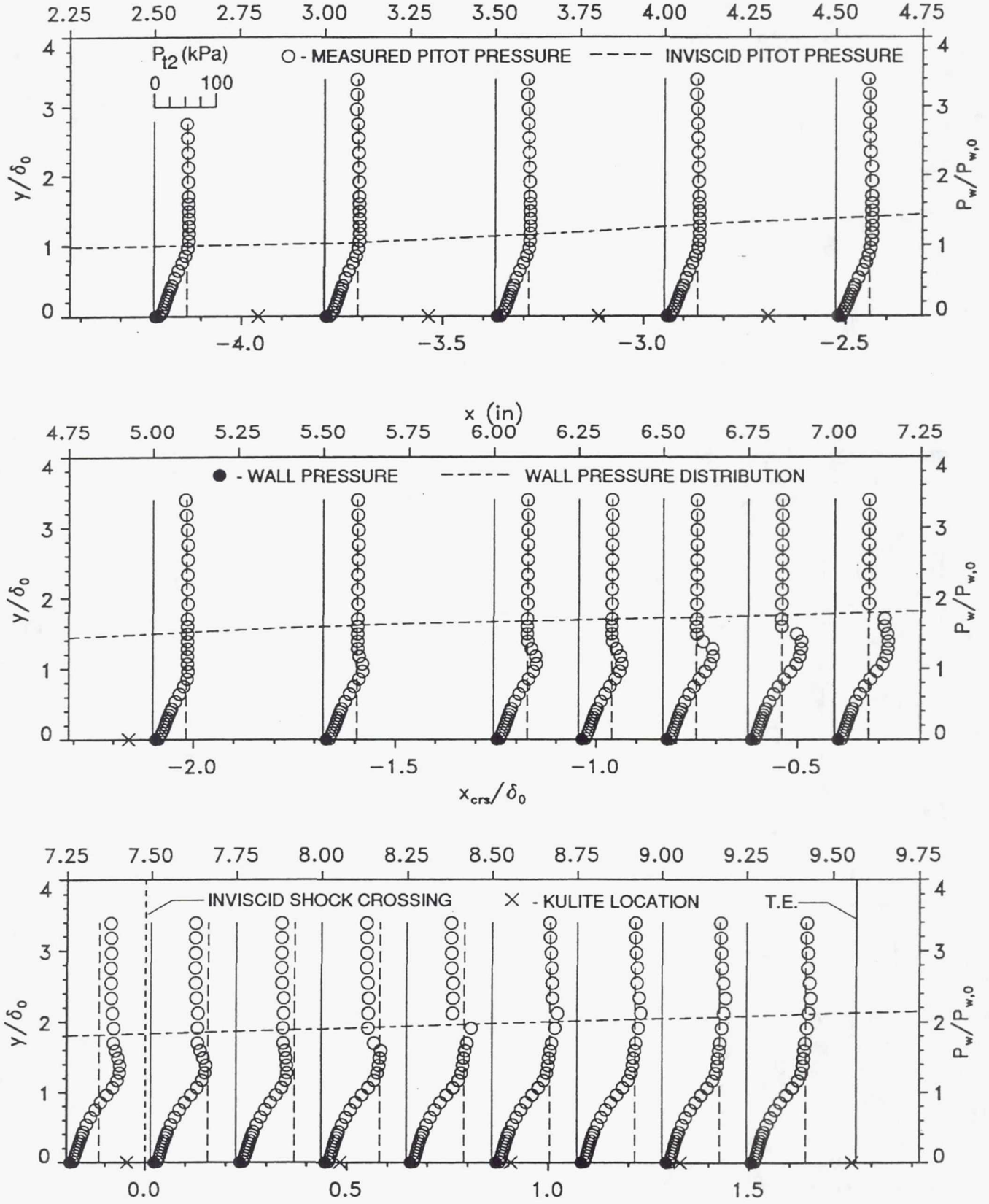

Fig. 6 Axial Pitot pressure profile development in the plane of symmetry (z=0), α=6°.

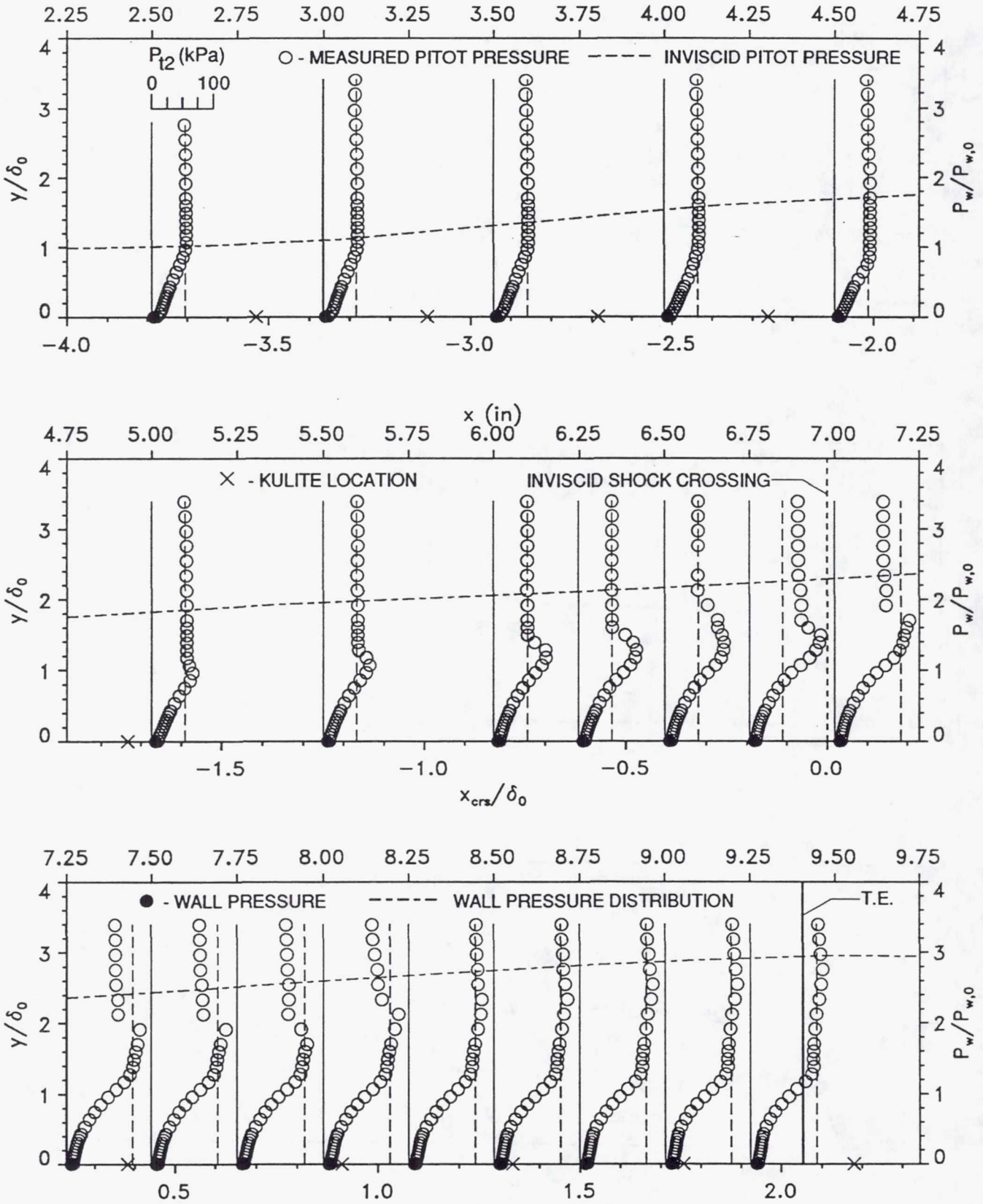

Fig. 7 Axial Pitot pressure profile development in the plane of symmetry (z=0), α=8°.

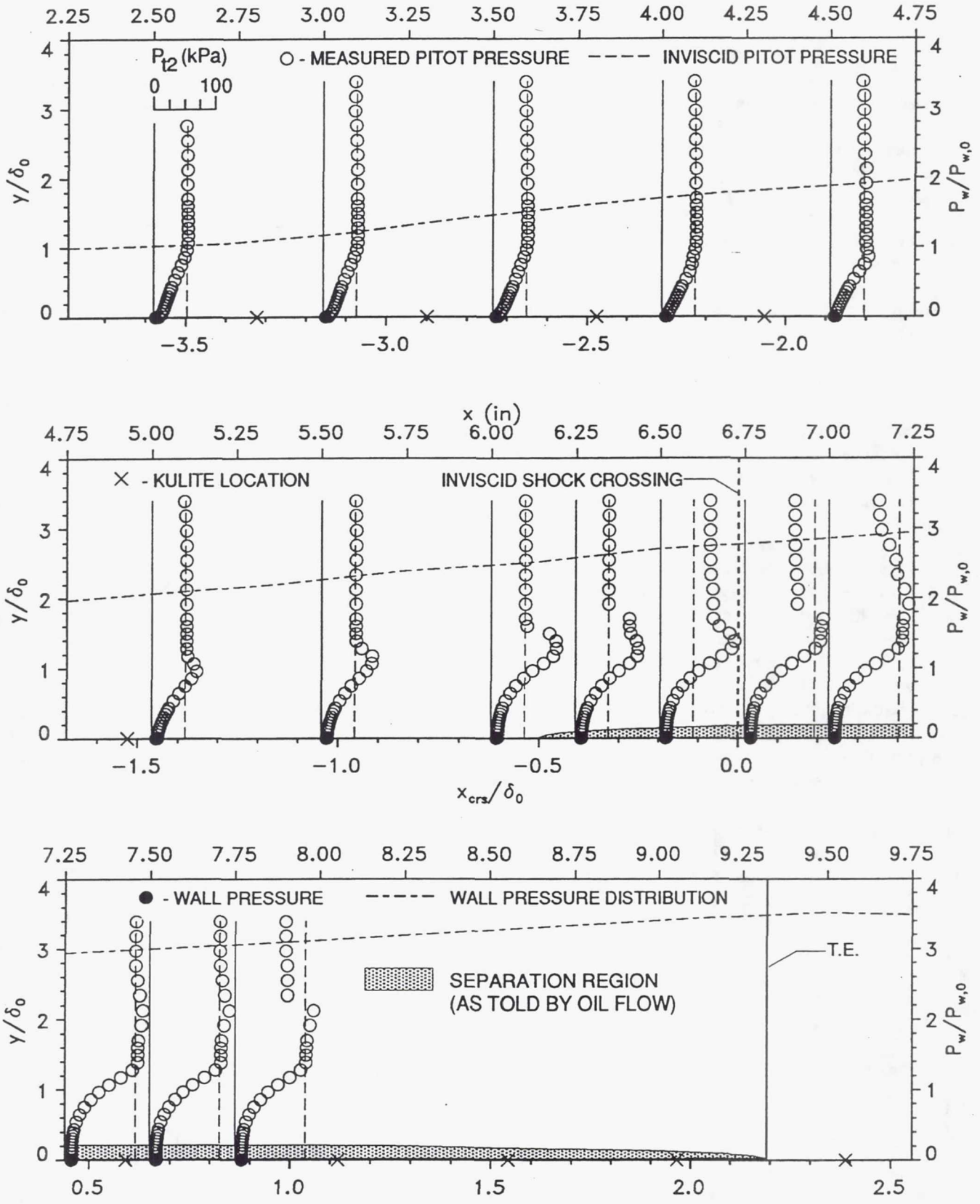

Fig. 8 Axial Pitot pressure profile development in the plane of symmetry (z=0), α=9°.

Fluctuating Surface Pressure

Limited unsteady surface pressure data in the plane of symmetry were measured with Kulite Model XCS-062 dynamic pressure transducers. Four transducers were mounted on a repositionable plate that could be installed in four different positions. During data reduction, it was determined that the mean output of one transducer was erratic and hence not used. Thus, at a given operating condition, pressure traces were recorded at a total of twelve streamwise locations on the centerline. These locations are indicated by the ×'s in Figs. 4, 6, 7 and 8. Unfortunately, the removal of the faulty transducer resulted in a rather large axial gap in the interaction region. All the Kulite data were obtained with the 22.9 cm generator plates.

The output from a transducer was amplified by a Preston amplifier Model 8300 XWB with a gain setting of 100. The amplified signal was then lowpass filtered at 50 kHz. The output of the filters was further amplified and offset via a Thermal Systems Inc. Model 157 signal conditioner. The gain and offset of the signal conditioner were adjusted for each data record so as to take full advantage of the ±5 volt input range of the A/D board. The signal conditioner output was digitized and recorded on a Concurrent Corporation data acquisition computer Model 5240. For all data records, the signal was sampled at 200 kHz/channel. The number of samples per channel was 204,800 resulting in a total sampling time of just over a second. A comparison between the mean Kulite output and the conventional wall pressure taps for a deflection angle of α=9° is shown in Fig. 9.

Wall static pressure RMS distributions in the plane of symmetry are shown in Fig. 10a normalized by upstream reference values and in Fig. 10b normalized by the local wall pressure. The left ordinate in in Fig. 10a is referenced to the undisturbed mean wall pressure and the right ordinate is referenced to the undisturbed RMS value. The upstream portion of the α=2° distributions are sufficiently removed from the interaction region so as to be representative of the undisturbed incoming boundary layer. The fluctuation intensity in this region is just under 1%. For deflection angles greater than 2°, the distributions exhibit a peak at the beginning of the interaction that coincides with the start of the mean pressure rise. For the strongest interaction considered (α=10°), the intensity rises very abruptly to a relatively high value. With reference to the upper right plot of Fig. 4, this high intensity was measured at the first Kulite location upstream of the separated region. The initial peak is followed by a decrease and then a second peak whose axial position varies with the deflection angle.

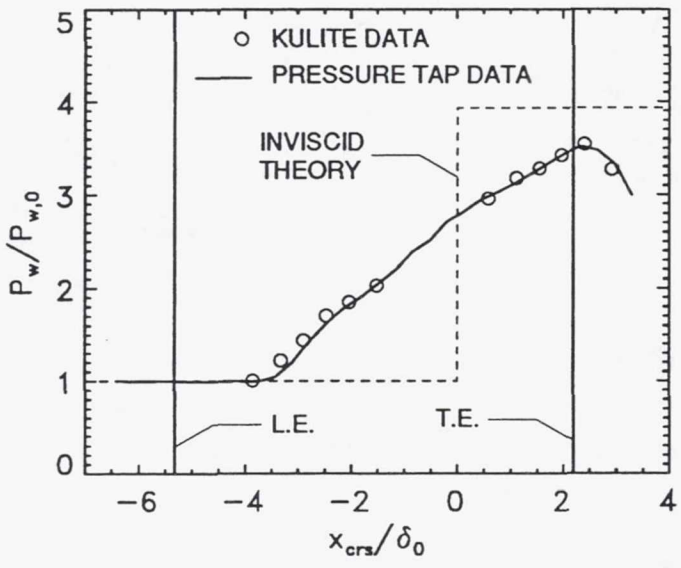

Fig. 9 Comparison between Kulite and wall tap mean pressure, α=9°, L_{gen}=22.9 cm.

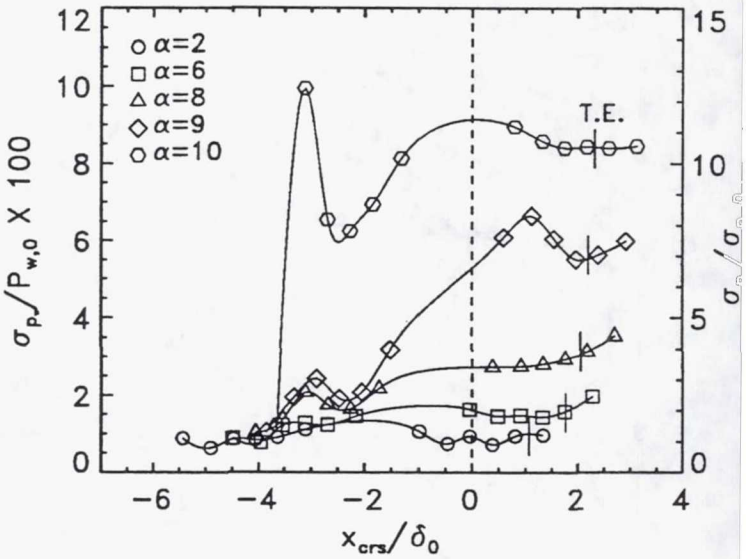

a) Normalized by undisturbed quantities.

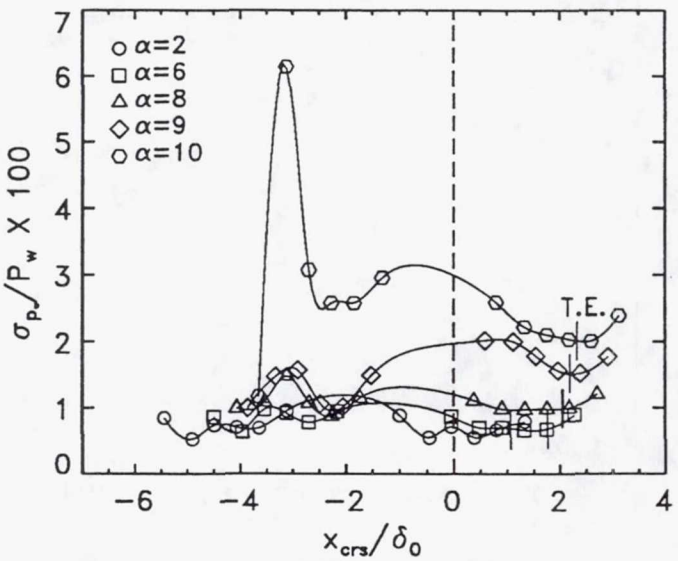

b) Normalized by local wall pressure.

Fig. 10 Wall pressure RMS distributions in the plane of symmetry, L_{gen}=22.9 cm.

The results in Fig. 10 may be compared with the Mach 2.96 data of Batcho *et al.*[2] Recall from Table 1 that the boundary layer thickness for this study is nearly an order of magnitude thinner than the present case. A comparison of the RMS pressure levels for the undisturbed boundary layer shows that they are virtually the same. Although the operating conditions are somewhat different, the α=7° and α=11° cases in Batcho's study are qualitatively similar to the α=6°and α=9° cases, respectively, of the present study. Quantitatively, the RMS levels for Batcho's α=7° case fall between the present α=6° and α=8° cases.

Normalized power spectral density functions corresponding to each of the data points in Fig. 10 were calculated and are shown in Fig. 11. Along the top of the plots, the streamwise location of the Kulite transducer relative to the upstream reference plane is denoted. The number in parentheses is a reference number used to distinguish between the three good transducers (transducer #3 was determined to be faulty). The transducers located at x=2.18, 2.81 and 3.31 inches for the α=2° case should be representative of the undisturbed incoming boundary layer. Each of these locations correspond to a different transducer. A notable difference between the three transducer outputs is the presence of several high frequency (f > 10kHz) spikes for transducers #2 and #4 which are not present for transducer #1. The source of this high frequency noise has been traced to individual channels of the data acquisition A/D board. Another feature common to all three transducers in the undisturbed spectrum plots is the presence of a large amplitude fluctuation at approximately 300 Hz. The source of this frequency is unknown, but some recent measurements made by Barnhart[15] in the NASA Lewis 1×1 SWT may shed some light as to their origin. As a component of his study of a blunt fin interaction, Barnhart recorded unsteady wall pressure traces for Mach 2, 3, 4 and 5 in the undisturbed boundary layer. Identical instrumentation was used with the exception of the second amplifier which in his study was a Pacific Instruments signal conditioner. For the Mach 2 case, Barnhart's data showed a very discrete spike at about 1kHz which, interestingly, all but disappeared when the tunnel mass flow rate was reduced. The second amplifier used in the present study was subsequently tested to determine if it was the source of the 300 Hz component. It was not. If this noise is truly a feature of the incoming flow it is puzzling as to what physically could create such a discrete frequency. Clearly, this issue must be resolved before any further measurements of this type are made.

Ignoring for the moment the noise components of the signals, the frequency content of the incoming boundary layer is fairly broadband with the dominant frequency between 2 to 3 kHz. With the exception of the α=10° case, the spectrum for the Kulite transducer located furthest upstream (x=2.18 in) is independent of the generator plate deflection angle. At α=10°, some influence of the separation shock is distinguishable in the spectrum. As the strength of the interaction is increased, the contribution of the noise components is diminished until at the strongest interaction considered (α=10°), they are negligible. For the α=6, 8, and 9° cases, moving through the interaction results in a slight shift in center frequency from the undisturbed value of ~2.5 kHz down to ~1.5 kHz. At the beginning of the α=10° interaction, there is a large shift in center frequency down to ~150 Hz (see x=2.81 in). This location corresponds to where the highest RMS fluctuations were observed and is the first Kulite location upstream from the separated region (see upper right plot in Fig. 4). The 150 Hz frequency can also be observed in the spectrum immediately downstream (x=3.31), but to a lessor degree. A similar low frequency component is also observed in the first data point upstream of the inviscid crossing shock location for Poddar's α=7° symmetric interaction. Surprisingly, this low frequency component was absent in Poddar's α=11° data, but this may be due to inadequate resolution of the region. Moving through the remainder of the interaction region, the spectrum for the α=10° case approaches a similar shape as the weaker interaction cases with one notable difference. The first pressure trace downstream of the inviscid shock crossing location (x=7.43 in) exhibits a second peak in the spectrum at about 10 kHz. A trace of this frequency component can also be seen in the spectrum immediately downstream (x=8.06 in). Unfortunately, the rather large axial gap in the data prevents complete assessment of this feature. Another feature of these results is the broadening of the spectrum as the shock crossing location is approached (see e.g., the distributions at x=4.93)., but again analysis is limited by the axial gap in the data.

Through most of the interaction region of the present study, the dominant frequencies have been observed to be centered in the range from 1 to 3 kHz, excluding the low frequency peak observed at the beginning of the α=10° interaction. In comparison, the Mach 3, thin boundary layer results of Poddar *et al.*[3] show dominant frequencies an order of magnitude higher. This difference is presumably related to the different length scales associated with the different boundary layer thicknesses.

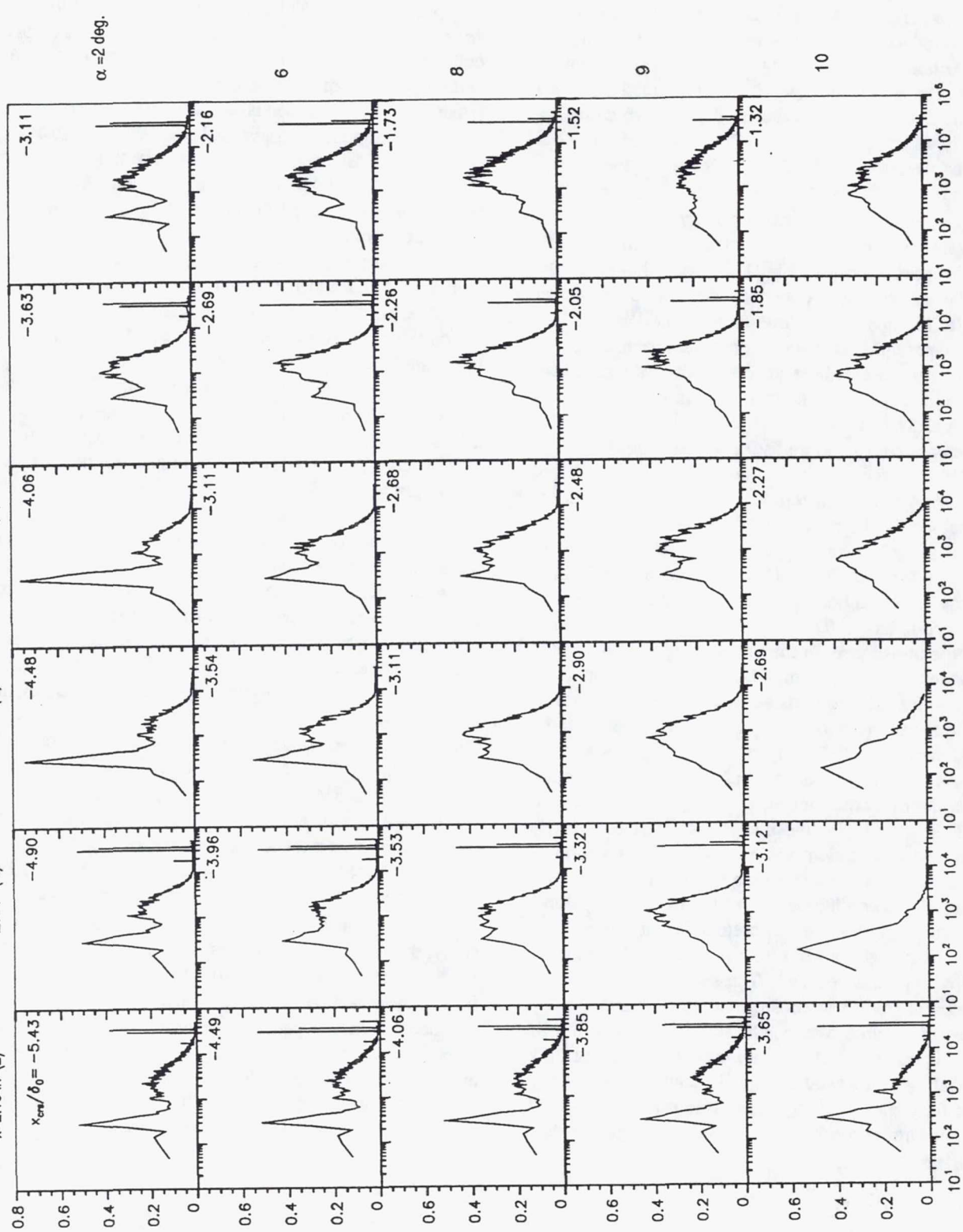

Fig. 11 Wall pressure power spectral densities in the plane of symmetry. (Continued . . .)

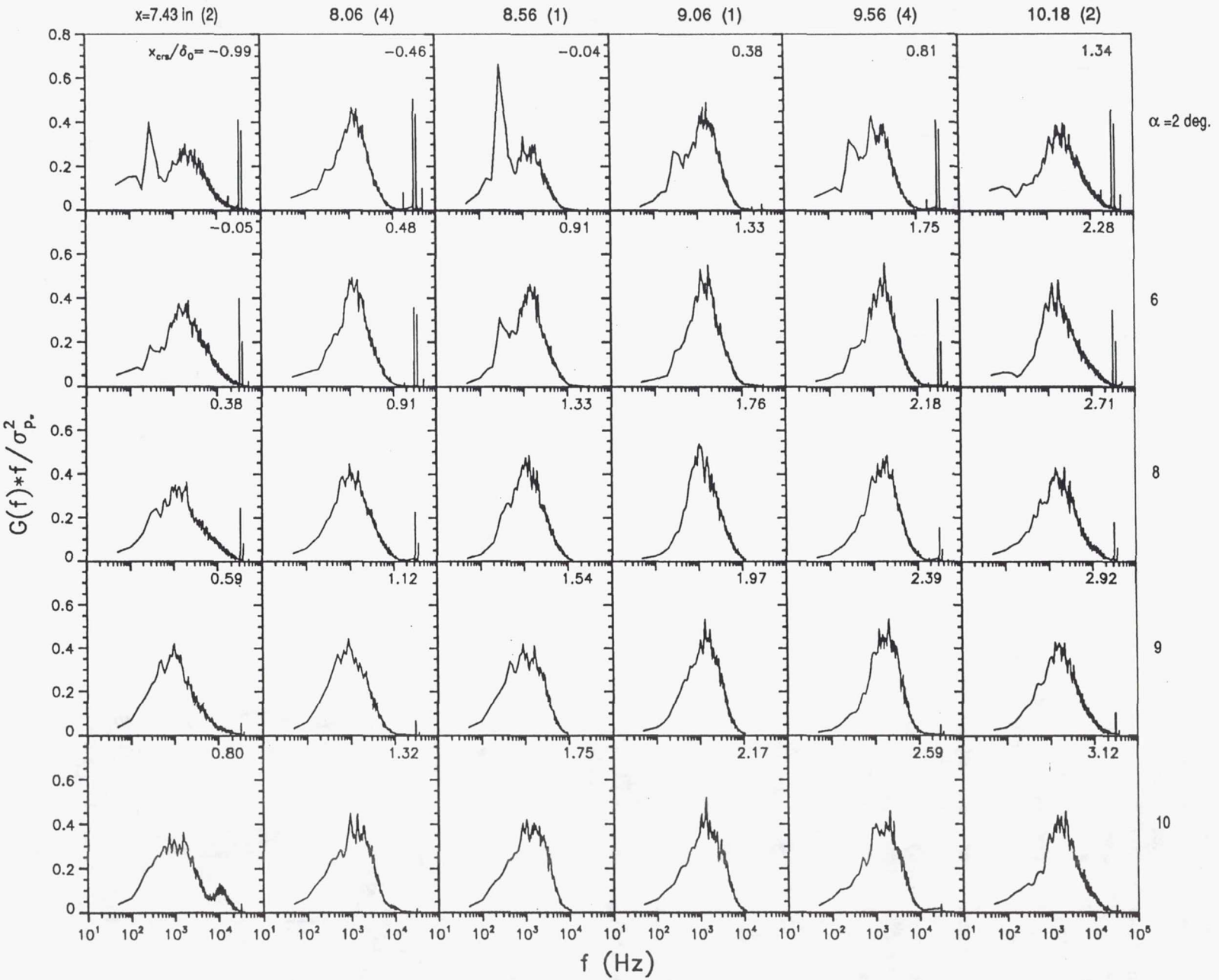

Fig. 11 Wall pressure power spectral densities in the plane of symmetry.

Pitot Pressure Contours

Pitot pressure surveys were conducted in the cross plane just upstream of the generator plate trailing edge plane. These measurements were made in a similar manner to the centerline profile surveys except that a flattened 3–hole Cobra probe was utilized. The measurement plane relative to the model geometry is shown in Fig. 12. Results of the surveys for α=6, 8 and 9° are shown in Fig. 13. In these plots, the local Pitot pressure is normalized by the undisturbed upstream value ($P_{t2,0}$ = 55 kPa). Probing at this location for the α=9° case was possible because the main body of the probe was in the expansion region downstream of the trailing edge. These data were taken in only one half of the facility and then imaged for presentation purposes.

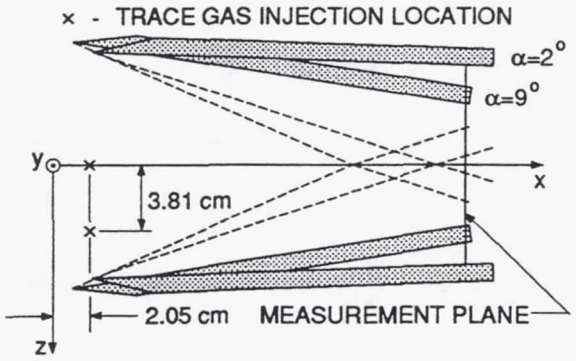

Fig. 12 Transverse measurement plane.

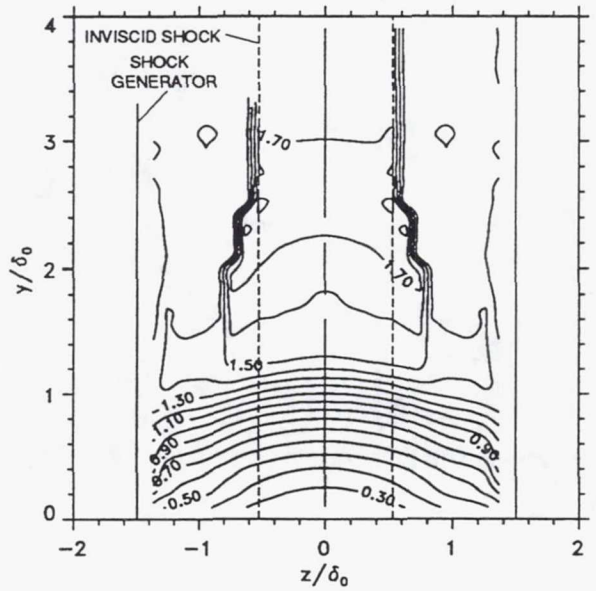

a) α = 6°.

Fig. 13 Pitot pressure distributions ($P_{t2}/P_{t2,0}$) at x = 9.25 in, L_{gen} = 22.9 cm. (Continued . . .)

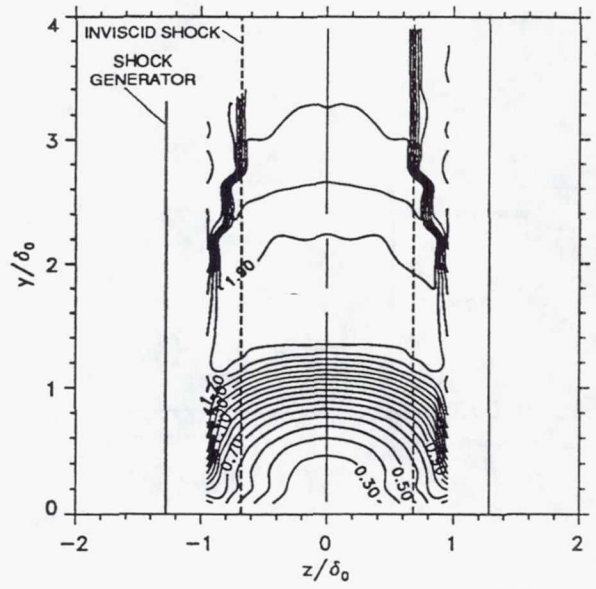

b) α = 8°.

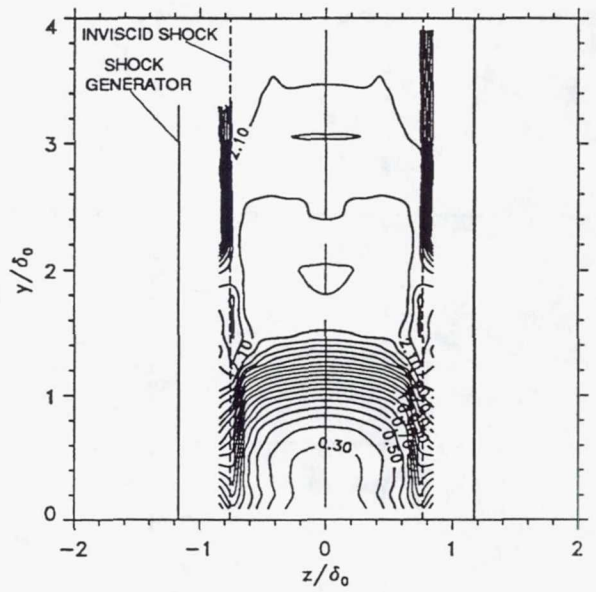

c) α = 9°.

Fig. 13 Pitot pressure distributions ($P_{t2}/P_{t2,0}$) at x = 9.25 in, L_{gen} = 22.9 cm.

In the core region of the flow, the measured shock location agrees fairly well with the inviscid theory. As the interaction region is approached from the core region (–y direction), the distance between the shocks increases. The lifting of the boundary layer leading to separation is clearly seen as the strength of the interaction is increased. The distortion of the contours is indicative of a pair of contra-rotating vortices centered about the plane of symmetry with common flow away from the floor surface. The presence of these vortices appears in previous calculations of the crossing shock configuration.[10]

Volume Fraction Contours

Near wall transport was investigated by means of a high speed trace gas technique recently developed by Reichert[16] and extended to supersonic flows by Davis and Hingst.[17]. The technique involves leaking pure ethylene through a static pressure port and then sampling the flow in a downstream plane. Sampling is done through a conventional Pitot tube and pumped into a flame ionization detector (Gow-Mac Model 23–500) hydrocarbon analyzer for analysis. The output from the analyzer is the local concentration of the ethylene-air mixture in ppm of ethylene. Ethylene was injected into the flow field from two locations. The location of the taps and the location of the measurement plane are shown in Fig. 12. Results for various deflection angles are shown for the centerline and offset injection in Fig. 14 and Fig. 15, respectively. For the centerline injection case, data were taken on only one side of the centerline and then imaged for presentation. The results are plotted in terms of the volume fraction normalized by the maximum volume fraction in the measurement plane for the $\alpha = 2°$ centerline injection case. The development of the ethylene plume is a function of both mean convection and turbulent diffusion. For the α=2° centerline injection case, the peak concentration occurs on the surface and the remaining distribution is primarily the result of turbulent diffusion. At α=6°, the peak concentration decreases by about 20% and has lifted from the surface by mean convection. The transverse width of the plume does not increase significantly over the α=2° case. At α=9°, the peak concentration decreases significantly and is lifted even further from the surface. The width of the plume has increased considerably indicating an substantial increase in turbulence intensity. An interesting aspect of these results is that the distributions do not have the characteristic horseshoe shape associated with the streamwise vortex structure that is implied by the Pitot pressure distributions.

Similar comments also apply to the offset injection case (Fig. 15), but here a greater degree of distortion of the plume is observed, particularly for the α=9° where the elongation in the y direction implies an upward flow along the generator plates. Fluid for the α=9° case migrates over to and even crosses the centerline, but again the contours near the centerline are not characteristic of the presence of a vortex pair.

Concluding Remarks

Surface and flowfield measurements in a symmetric crossing shock/turbulent boundary layer interaction have been presented. From the results, the following conclusions can be made:

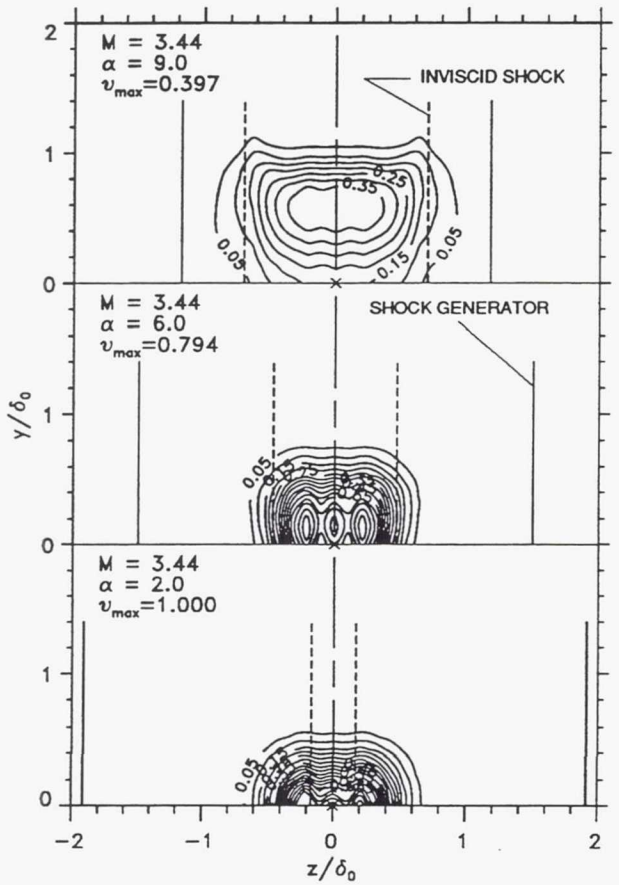

Fig. 14 Volume fraction distributions for M = 3.5, α = 2°, 6° and 9° cases, centerline injection.

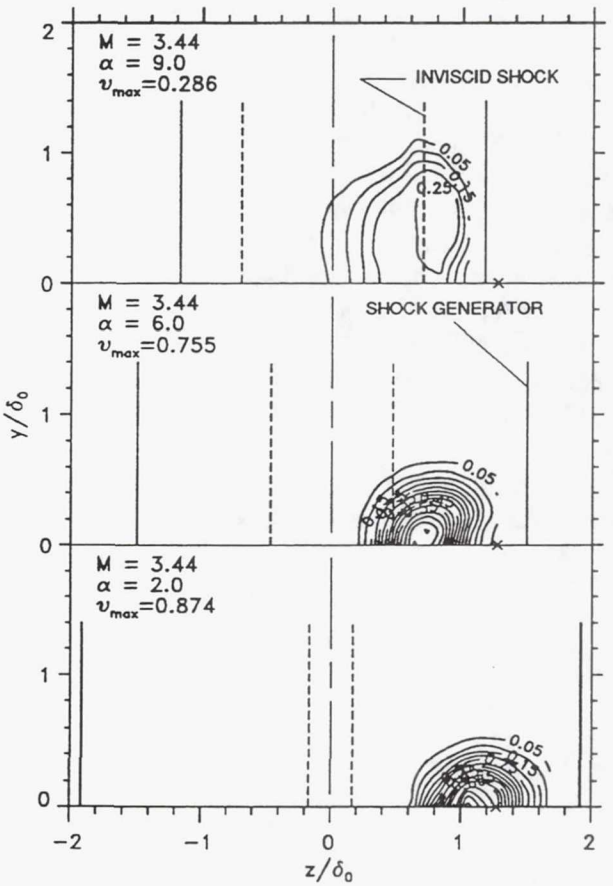

Fig. 15 Volume fraction distributions for M = 3.5, α = 2°, 6° and 9° cases, offset injection.

1) The length of the generator plate has a significant effect on the strength of the interaction for a given deflection angle. More specifically, the distance from the shock crossing location to the trailing edge expansion region must be large relative to the incoming boundary layer thickness in order to capture the true strength of the interaction.

2) A qualitative difference is observed in the surface pressure distributions depending on whether or not a gross separation of the flow occurs. This feature may be useful in detecting flow separation when only surface pressure is available.

3) Preliminary dynamic surface pressure measurements indicate, like previous studies, a significant unsteady characteristic in the interaction region. The dominant frequencies are generally centered around 1 kHz. For the strongest interaction considered, a high amplitude unsteadiness that occurs at $\sim$150 Hz was detected. The undisturbed boundary layer power spectrum indicate the need for more extensive documentation of the acoustic properties of the NASA Lewis 1$\times$1 SWT.

4) Pitot pressure measurements illustrate the development of the boundary layer through the interaction region and should be useful for CFD validation.

References

[1] Mee, D. J., Stalker, R. J., and Stollery, J. L., "Glancing Interactions Between Single and Intersecting Oblique Shock Waves and a Turbulent Boundary Layer," *Journal of Fluid Mechanics*, Vol. 170, 1986, pp. 411–433.

[2] Batcho, P. F., Ketchum, A. C., Bogdonoff, S. M., and Fernando, E. M., "Preliminary Study of the Interactions Caused by Crossing Shock Waves and a Turbulent Boundary Layer," AIAA Paper 89-0359, 1989.

[3] Poddar, K. and Bogdonoff, S. M., "A Study of Unsteadiness of Crossing Shock Turbulent Boundary Layer Interactions," AIAA Paper 90-1456, 1990.

[4] Hingst, W. R. and Williams, K. E., "Interaction of Two Glancing, Crossing Shock Waves with a Turbulent Boundary Layer at Various Mach Numbers," NASA TM 103740, 1991.

[5] Williams, K. E. and Hingst, W. R., "The Effect of Varing Mach Number on Crossing, Glancing Shocks / Turbulent Boundary Layer Interactions," AIAA Paper 91-2157, 1991.

[6] Garrison, T. J. and Settles, G. S., "Flowfield Visualization of Crossing Shock-Wave/Boundary-Layer Interactions," AIAA Paper 92-0750, 1992.

[7] Kussoy, M. I. and Horstman, K. C., "Intersecting Shock-Wave/Turbulent Boundary-Layer Interactions at Mach 8.3," NASA TM 103909, 1992.

[8] Gaitonde, D. and Knight, D., "Numerical Experiments on the 3-D Shock Wave-Boundary Layer Interaction Generated by a Sharp Fin," AIAA Paper 88-0309, 1988.

[9] Gaitonde, D. and Knight, D., "Numerical Investigation of Some Control Methods for 3-D Turbulent Interactions Due to Sharp Fins," AIAA Paper 89-0360, 1989.

[10] Narayanswami, N., Knight, D., Bogdonoff, S. M., and Horstman, C. C., "Crossing Shock Wave-Turbulent Boundary Layer Interactions," AIAA Paper 91-0649, Jan. 1991.

[11] Baldwin, B. S. and Lomax, H., "Thin Layer Approximation and Algebraic Model for Separated Turbulent Flows," AIAA Paper 78-257, 1978.

[12] Jones, W. and Launder, B., "The Prediction of Laminarization with a Two-Equation Model of Turbulence," *Int. Journal of Heat and Mass Transfer*, Vol. 15, 1972, pp. 301–304.

[13] Reddy, D. R., "3-D Navier-Stokes Analysis of Crossing, Glancing Shocks/Turbulent Boundary Layer Interactions," AIAA Paper 91-1758, 1991.

[14] Sun, C. C. and Childs, M. E., "A Modified Wall-Wake Velocity Profile for Turbulent Compressible Boundary Layers," *Journal of Aircraft*, Vol. 10, June 1973, pp. 381–383.

[15] Barnhart, P. , Sverdrup Technology, Cleveland, OH (private communication).

[16] Reichert, B. A., *A Study of High Speed Flows in an Aircraft Transition Duct*, Ph.D. Dissertation, Iowa State University, Ames, Iowa, 1991. (also NASA TM 104449).

[17] Davis, D. O., Hingst, W. R., and Porro, A. R., "Experimental Investigation of a Single Flush-Mounted Hypermixing Nozzle," AIAA Paper 90-5240, 1990. (also NASA TM 103726).

REPORT DOCUMENTATION PAGE

Form Approved
OMB No. 0704-0188

1. AGENCY USE ONLY (*Leave blank*)	2. REPORT DATE	3. REPORT TYPE AND DATES COVERED
	June 1992	Technical Memorandum

4. TITLE AND SUBTITLE

Surface and Flow Field Measurements in a Symmetric Crossing Shock Wave/Turbulent Boundary-Layer Interaction

5. FUNDING NUMBERS

WU–505–62–52

6. AUTHOR(S)

D.O. Davis and W.R. Hingst

7. PERFORMING ORGANIZATION NAME(S) AND ADDRESS(ES)

National Aeronautics and Space Administration
Lewis Research Center
Cleveland, Ohio 44135–3191

8. PERFORMING ORGANIZATION REPORT NUMBER

E–7716

9. SPONSORING/MONITORING AGENCY NAMES(S) AND ADDRESS(ES)

National Aeronautics and Space Administration
Washington, D.C. 20546–0001

10. SPONSORING/MONITORING AGENCY REPORT NUMBER

NASA TM–106086
AIAA–92–2634

11. SUPPLEMENTARY NOTES

Prepared for the 10th AIAA Applied Aerodynamics Conference sponsored by the American Institute of Aeronautics and Astronautics, Palo Alto, California, June 22–24, 1992. D.O. Davis and W.R. Hingst, NASA Lewis Research Center. Responsible person, David O. Davis, (216) 433–8116.

12a. DISTRIBUTION/AVAILABILITY STATEMENT

Unclassified - Unlimited
Subject Category

12b. DISTRIBUTION CODE

13. ABSTRACT ***(Maximum 200 words)***

Results of an experimental investigation of a symmetric crossing shock/turbulent boundary layer interaction are presented for a Mach number of 3.44 and deflections angles of 2, 6, 8, and 9°. The interaction strengths vary from weak to strong enough to cause a large region of separated flow. Measured quantities include surface static pressure (both steady and unsteady) and flowfield Pitot pressures. Pitot profiles in the plane of symmetry through the interaction region are shown for various deflection angles. Oil flow visualization and the results of a trace gas streamline tracking technique are also presented.

14. SUBJECT TERMS

Supersonic flow; Turbulent boundary layer; Crossing oblique shock waves; Shockwave interaction; Symmetry

15. NUMBER OF PAGES

20

16. PRICE CODE

A03

17. SECURITY CLASSIFICATION OF REPORT	18. SECURITY CLASSIFICATION OF THIS PAGE	19. SECURITY CLASSIFICATION OF ABSTRACT	20. LIMITATION OF ABSTRACT
Unclassified	Unclassified	Unclassified	